On the onset of the ice phase in boundary layer Arctic clouds

Jean-François Gayet, Renate Treffeisen, Alfred Helbig, Jörg Bareiss, Atsushi Matsuki, Andreas Herber, Alfons Schwarzenboeck

To cite this version:

Jean-François Gayet, Renate Treffeisen, Alfred Helbig, Jörg Bareiss, Atsushi Matsuki, et al.. On the onset of the ice phase in boundary layer Arctic clouds. Journal of Geophysical Research, 2009, 114 (D19), 10.1029/2008jd011348 . hal-01981212

JOURNAL OF GEOPHYSICAL RESEARCH, VOL. 114, D19201, doi:10.1029/2008JD011348, 2009

On the onset of the ice phase in boundary layer Arctic clouds

Jean-François Gayet,[1] Renate Treffeisen,[2] Alfred Helbig,[3] Jörg Bareiss,[3] Atsushi Matsuki,[4] Andreas Herber,[2] and Alfons Schwarzenboeck[1]

Received 22 October 2008; revised 29 May 2009; accepted 9 June 2009; published 1 October 2009.

[1] Airborne measurements in slightly supercooled Arctic boundary layer stratocumulus have been carried out in Spitsbergen on 29 May during the ASTAR 2004 campaign. Cloud measurements have been performed in both warm and cold sectors of a cold front passing the observation area. The results show a north–south gradient in freezing properties and thus evidence of significant differences in the cloud microstructure. Ahead of the front line, in the warm sector (cloud top temperature at $-4°$C), no ice particles were detected. The cloud formed in clean air conditions (aerosol concentration of 300 cm^{-3}) with subsequent large effective diameter (20–26 μm) and low concentration (50 cm^{-3}) of cloud droplets. Therefore, the collision-coalescence process was effective, favoring the drizzle formation with concentration up to 300 L^{-1} ($D > 50$ μm). In the cold sector behind the front, with a lower cloud top temperature ($-6°$C), ice crystals were observed in the entire cloud layer, and no droplets larger than about 50 μm (drizzle) were detected. The observations confirm high ice particle concentrations (up to 50 L^{-1}) even with rather warm cloud top ($-6°$C) compared to previous studies in Arctic clouds. The shattering of isolated drops during freezing and the ice splinter production during riming appear to be the most likely processes to explain the observations of high ice concentration in the cold sector. Analysis of back trajectories did not reveal significant differences in the origin of the air masses in the warm and cold sectors that might have contributed to the differentiation of aerosol composition and thus cloud properties. A cloud top temperature colder than $-4°$C appears to be required for the onset of the ice phase in this slightly supercooled stratiform cloud.

Citation: Gayet, J.-F., R. Treffeisen, A. Helbig, J. Bareiss, A. Matsuki, A. Herber, and A. Schwarzenboeck (2009), On the onset of the ice phase in boundary layer Arctic clouds, *J. Geophys. Res.*, *114*, D19201, doi:10.1029/2008JD011348.

1. Introduction

[2] There is ever increasing evidence that the global climate is changing and nowhere it is more strongly expressed than in the polar region. Observations, consistent with model simulations, show that the Arctic is warming twice as much as the global average [*Arctic Climate Impact Assessment*, 2004]. However, the impacts of climate change in the polar region are also likely to have profound global impacts. Model runs also indicate the importance of interactions with the lower latitudes through complex teleconnection and dynamic patterns [e.g., *Dethloff et al.*, 2006]. The latest report of the Intergovernmental Panel on Climate Change [*Intergovernmental Panel on Climate Change (IPCC)*, 2007] pointed out that the role of atmospheric aerosols and clouds in the climate system remains very uncertain. High-latitude cloud interactions are determinant factors to global climate by several issues [*Curry et al.*, 1996]: the impact of cloud-radiation processes on the stability of Arctic Ocean pack ice [*Curry et al.*, 1993]; the impact of high-latitude precipitation on both the global ocean thermohaline circulation [*Dickson et al.*, 2002] and on Arctic ice growth or shrinkage and subsequent effects on global sea level [*IPCC*, 2007]; and potential thawing of the permafrost soils that could release tremendous stores of carbon to the atmosphere [*Cappelaz et al.*, 1993].

[3] Cloud-radiation interactions and subsequent effects on Arctic climate system are very complex because of the high surface albedo of Arctic ice and snow sheets, the low Sun elevation in this region for a large time of the year [*Curry et al.*, 1996], and a frequent occurrence of mixed phase clouds with optical properties deviating from those of liquid clouds [*Hobbs and Rangno*, 1998; *Verlinde et al.*, 2007]. The cloud radiative properties are determined by cloud microphysical properties which include: the liquid/ice water content, the size and shape of the cloud particles and the phase of the particles (cloud droplets and/or ice crystals).

[4] The cloud formation and the cloud characteristics crucially depend on the properties of aerosol particles which act like cloud condensation nuclei (*CCN*) and ice

---

[1] Laboratoire de Météorologie Physique, UMR 6016, Université Blaise Pascal, CNRS, Aubière, France.

[2] Alfred Wegener Institute for Polar and Marine Research, Bremerhaven, Germany.

[3] Department of Environmental Meteorology, University of Trier, Trier, Germany.

[4] Frontier Science Organization, Kanazawa University, Kanazawa, Japan.

0148-0227/09/2008JD011348

forming nuclei (*IN*) [*Sassen*, 2005]. Because boundary layer Arctic clouds often contain low droplet concentration (i.e., < 100 cm^{-3}) [see, e.g., *Hobbs and Rangno*, 1998; *Rangno and Hobbs*, 2001; *Zuidema et al.*, 2005], they are particularly vulnerable to modification of CCN properties [*Hegg et al.*, 1996; *Lubin and Vogelmann*, 2006]. Therefore, nucleation processes are still part of the open questions for modeling studies [*Morrison et al.*, 2005]. On the basis of well-documented observations in mixed phase clouds during M-PACE experiment [*McFarquhar et al.*, 2007] the discrepancy between the observed ice nuclei (IN) and ice crystal concentrations leads to significant model underprediction of crystal concentration [*Morrison et al.*, 2008] which is suggestive of missing ice initiation processes in current models (see discussion by *Fridlind et al.* [2007]).

[5] The Arctic cloud properties are difficult to retrieve from satellite remote sensing because the largest errors in ISCCP (International Satellite Cloud Climatology Project) cloud climatology occur in the polar region [*Rossow et al.*, 1993]. Since the recent active remote observations from space (for instance CALIPSO [*Winker and Trepte*, 2007]) much more detailed cloud observations are now available, but improvements in satellite retrievals are hampered by the lack of validation data. Since clouds in general have a wide variety of physical characteristics, detailed and more extensive measurements are one of the key requirements to increase our knowledge of the complex interactions between different physical processes and may serve as a basis for the development of more accurate microphysical and radiation parameterizations for regional Arctic climate models.

[6] In this paper we present the results from cloud observations carried out onboard the Polar2 aircraft operated by the Alfred Wegener Institute for Polar and Marine Research (AWI) obtained on 29 May 2004 during the ASTAR 2004 field experiment [e.g., *Engvall et al.*, 2008]. The flight was carried out over the Greenland Sea in the vicinity of the west coast of the Svalbard Archipelago. The main focus here is to use results of the cloud in situ measurements to characterize properties of slightly supercooled Arctic boundary layer stratocumulus clouds. The aircraft measurements are presented with a detailed analysis of the weather situation which belongs to them.

2. Instrumentation and Flight Procedure

2.1. Instrumentation

[7] The experimental campaign ASTAR (Arctic Study on Tropospheric Aerosol and Radiation) was carried out between 15 May and 19 June 2004, employing two specially equipped Dornier 228–101 aircrafts (Polar2 and the Polar4) of the Alfred Wegener Institute of Polar and Marine Research (AWI). Both research aircraft were equipped with meteorological probes for measurements of basic meteorological parameters along the flight track. Air temperature measurements were made with a Rosemount total temperature probe located above the nose of the fuselage. The static air temperature is calculated with an uncertainty better than ± 0.5 K. Because the liquid water content remained lower than about 0.6 g/m^3 during most of the ASTAR flights, no significant effects on the reliability of the temperature measurements were observed during cloud traverses.

[8] The instruments used for the determination of microphysical and optical properties of Arctic clouds on the Polar2 included four independent techniques: (1) the Polar Nephelometer, (2) the PMS 2D-C, (3) the Cloud Particle Imager (CPI), and (4) the Nevzorov probe. The combination of these techniques provides a description of particles within a diameter range varying from a few micrometers (typically 3 μm) to about two millimeters.

[9] Before the description of the instruments used in this study, we underline that the accuracies on cloud measurements might seriously be hampered by the shattering of ice crystals on probes with shrouded inlet (Polar Nephelometer, CPI and PMS 2D-C for instance) [*Korolev and Isaac*, 2005; *Heymsfield*, 2007; *McFarquhar et al.*, 2007]. For particle diameters larger than about 100 μm, the number of shattered particles increases with the concentration of large particles. Techniques have been proposed by *Field et al.* [2006] to separate real and artifact-shattered crystals from information of ice particle interarrival times making objective corrections possible. We note this technique was originally proposed by *Cooper* [1977]. New particle image probes with high pixel resolution may also be used to quantify the contribution of shattering to the particle size distributions and optical properties [*Lawson et al.*, 2006], however, these instruments were not available for the present study. The possible effects of ice crystal shattering on the present study will be discussed together with the results below.

[10] The Polar Nephelometer [*Gayet et al.*, 1997] measures the scattering phase function of an ensemble of cloud particles (i.e., water droplets or ice crystals or a mixture of these particles ranging from a few micrometers to about 1 mm diameter). Direct measurement of the scattering phase function allows particle types (water droplets or ice crystals) to be distinguished and calculations of the optical parameters to be performed (extinction coefficient and asymmetry parameter [see *Gayet et al.*, 2002a]). The accuracies on extinction coefficient and asymmetry parameters derived from the Polar Nephelometer are estimated to be within 25% and 4%, respectively [*Gayet et al.*, 2002a]. These accuracies could be affected by ice crystal shattering on the probe inlet.

[11] The PMS 2D-C instrument was also installed on the Polar2 aircraft. Because of some intermittent failures which occurred on the data acquisition system, the available data are not discussed in this study but have been used to validate the CPI measurements (see Appendix A). The PMS 2D-C probe provides information on particle size and shape for the size range 25–800 μm and the method of data processing has already been described in detail by *Gayet et al.* [2004]. The effects of the ice particle shattering on microphysical measurements are dependent on the conditions in which those measurements were performed. Referring to the results from *Field et al.* [2006], the ice particle concentration (from the 2D-C probe) could be overestimated by a factor of 4 where mass-weighted mean size is in excess of 3 mm. Because the mean volume diameter does not exceed 0.37 mm in our study (see Figure 5d) the effects should likely be much lower and the subsequent errors are expected to be within the usual (and large) uncertainties on particle concentration (75% [see *Gayet et al.*, 2002b]). Similar conclusions may be expected for CPI measurements (see below).

[12] The CPI registers cloud particle images on a solid-state, one-million-pixel digital charge-coupled device (CCD) camera by freezing the motion of the particle using a 40 ns pulsed, high-power laser diode [*Lawson et al.*, 2001]. A particle detection system (PDS) with upstream lasers precisely defines the focal plane so that at least one particle in the image is in the focus. Each pixel in the CCD camera array has an equivalent size in the sample area of 2.3 μm, so particles of sizes from approximately 10 μm to 2 mm are imaged. The shadow depth of each pixel can be expressed in up to 256 gray levels and the refresh rate of the CCD camera is of 40 Hz. A video-processing tool identifies and sizes particles within the one-million-pixel array, saving only the regions of interest. The CPI images were processed using the software [*Lefèvre*, 2007] developed at the Laboratoire de Météorologie Physique (LaMP). This software is based on the features and algorithms outlined in the manual of the original CPI view software [see *Lawson et al.*, 2001; *Baker and Lawson*, 2006] (CPIview CPI data processing software, SPEC Incorporated Boulder, Colorado, 2005, http://www.specinc.com/publications/CPIview_Manual.pdf). Moreover, it provides additional information on the ice particle morphology that is not available from the CPI view software. We note in passing the LaMP software uses the method proposed by *Lawson and Baker* [2006] for the determination of the ice water content from two-dimensional particle imagery. As indicated above the CPI data were used in order to derive the particle size distributions and the microphysical parameters as *Gallagher et al.* [2005] in cirrus clouds. The method of calibration of the CPI is described in Appendix A with some results of comparison with the 2D-C. The resulting uncertainties on derived microphysical parameters are found of the same order of the 2D-C, i.e., 75% and 100% on particle concentration and ice water content, respectively.

[13] The Nevzorov liquid water content (LWC) and total water content (TWC) instrument is a constant temperature hot-wire probe designed for aircraft measurements of the liquid and ice water content of clouds [*Korolev et al.*, 1998]. It consists of two separate sensors for measurements of cloud liquid and total (ice plus liquid) water content, giving two linear equations for the variables LWC and IWC to be solved. The accuracies on these quantities have been evaluated to 15% and 20% [*Korolev et al.*, 1998]. The accuracy on LWC measurements could be affected (underestimation) when large droplets (drizzle) are sampled. The results presented below consider only the LWC measurements. The IWC data were not reliable because of a bad setting of the "out-of-cloud" offset signal (negative nonrecorded value).

2.2. Flight Procedure

[14] The observations discussed in this paper were obtained during the Polar2 flight on 29 May 2004 between 1400 and 1700 UT over the Greenland Sea in the vicinity of the west coast of the Svalbard as displayed in Figure 1. Figure 1 represents the visible image of the Terra/MODIS satellite (Moderate-Resolution Imaging Spectroradiometer) at 1555 UT and gives an overview of the cloud situation with the locations of Ny-Ålesund and Longyearbyen (airport). The black solid line represents the flight trajectory along the airborne observations have been carried out. The flight pattern of Polar2 consisted of transects between two fixed way points A and B (see Figure 1) with vertical profiles through the cloud layer performed in the northern and southern ends of the A-B segment. The first vertical profile was obtained in the southern part (near point A) between 1450 and 1505 UT. The second vertical profile was performed in the northern part (near point B) between 1532 and 1550 UT and a third profile was carried out again in the southern region between 1555 and 1605 UT. All the cloud vertical profiles were carried out along ramped legs. We mention that the Polar4 aerosol measurements were conducted along the same flight track of Polar2 trough the cloud but with a time difference of around half an hour. We will discuss first the weather situation observed during the flight period as this is a major basis for understanding the observed processes.

3. Description of the Weather Situation on 29 May 2004

[15] The cloud characteristics measured over the Greenland Sea along the west coast of Svalbard took place within a low-pressure system and the associated flow pattern and cloud field. This low-pressure system moved from 27 to 31 May from north Greenland over Svalbard to southeast embedded in a general zonal flow pattern in the lower troposphere. Figure 2a (1200 UT) and Figure 2b (1800 UT) display the meteorological situation on 29 May at 925 hPa and represent geopotential, wind vector and potential temperature fields obtained from ECMWF analysis. The area of the airborne observations is indicated by a solid black line. At 1200 UT a low-pressure system is located at the position 80°N/8°E (Figure 2a). The trough line spans from the low center toward 7°E in relation to the geographical location of Ny-Ålesund. In the investigation area, the direction of the isobaric field cause an air mass flow from southwest and the potential temperature roughly follows the 270 K isotherm. Northward to Ny-Ålesund the horizontal distribution of the potential temperature indicates a distinct border of the cold air mass from NW with a value of 268 K. From 1200 UT until 1800 UT the low-pressure system moves eastward approximately 350 km to the position 79°N/26°E. At 1800 UT the cold front is situated at the east coast of Svalbard around 19°E to 17°E (Figure 2b). At that time in the investigation area the isobaric field causes the cold air mass flow oriented between 300° and 310° and the isotherms run parallel to the isohypses.

[16] However, from these weather charts the position of the cold front, passing the flight operation area between 1200 UT and 1800 UT, cannot be derived precisely enough in time for the interpretation of cloud in situ measurements discussed in section 4. Therefore, we considered meteorological observations from Ny-Ålesund and Zeppelin Mountain stations in order to estimate the time position of the front. We note the Mount Zeppelin station is located in the close vicinity of Ny-Ålesund (see Figure 1) at 475 m elevation [*Engvall et al.*, 2008]. All meteorological observations, especially the tendency of surface barometric pressure, indicate for Ny-Ålesund the passage of the cold front around 1300 UT. In connection the wind direction changes from 110° at 1200 UT to 230° at 1300 UT and finally at 1600 UT from 270° to 300°. The wind velocity shifts from 7 m/s at 1300 UT to 8.5 m/s at 1800 UT. The air temperature

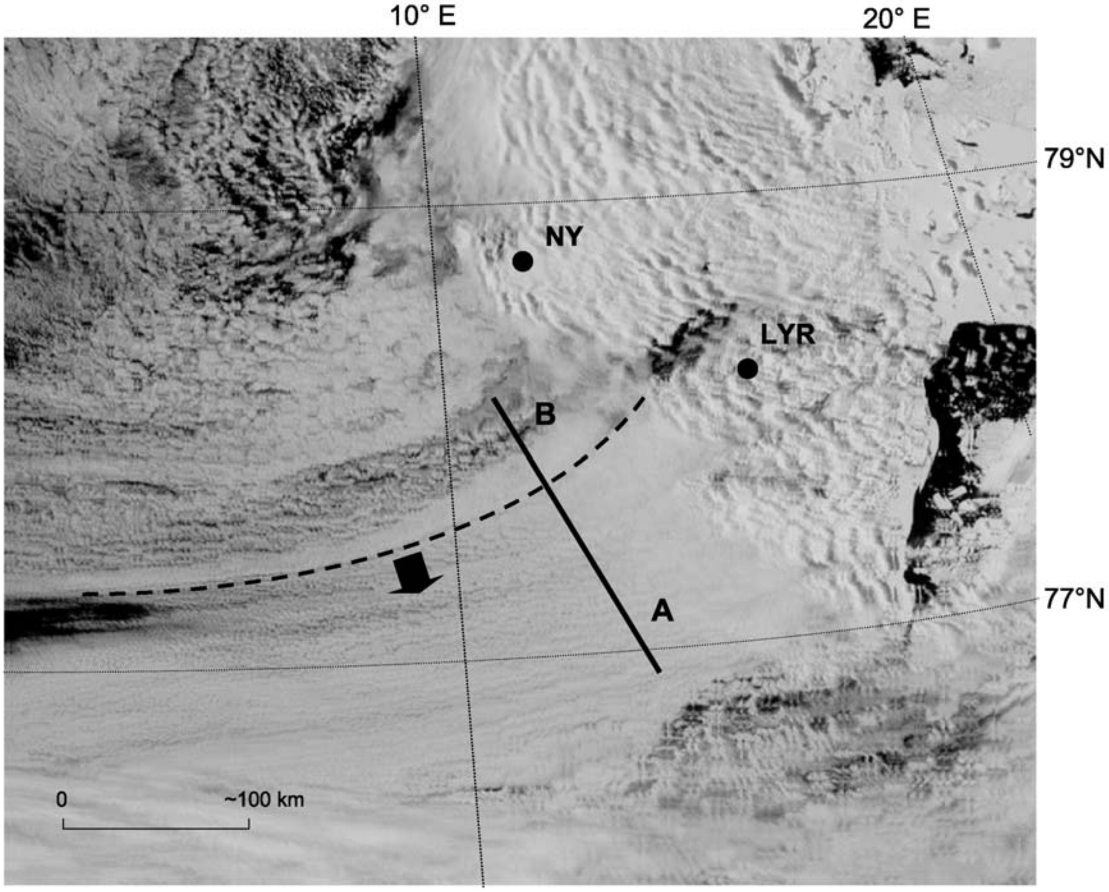

Figure 1. Satellite picture taken on 29 May at 1555 UT by Terra/MODIS (visible channel). The Polar2 flight trajectory between the way points A and B is superimposed to the satellite picture (solid black line). NY and LYR are the locations of Ny-Ålesund and Longyearbyen, respectively. The dashed line represents the approximate position of the cold front at 1555 UT.

drops very fast from 2.9°C at 1230 UT to about −0.7°C at 1500 UT. Information about precipitation was obtained by analyzing ground-based Lidar observations which showed a slight precipitation from 0700 and 1000 UT and heaviest precipitation at 1300 UT when the cold front passed.

[17] In order to identify in which air mass the Polar2 measurements were performed, one has to consider the movement of the cold front. On the basis of Terra/MODIS satellite image (visible channel) at 1555 UT (see Figure 1) the cold front line may be roughly identified by analyzing changes in the cloud structure. The observation area is characterized by a rather uniform boundary layer stratiform cloud system ahead of the cold front whereas rather scattered cloudiness can be seen at the rear. A simple time location scheme has been used to determine the position of the leading edge of the cold air mass (drifting from NW into the flight operation area). Assuming a front line with the known location at Ny-Ålesund around 1300 UT, a movement direction of 140° with a velocity of about 32 km/h derived from the two successive Terra/MODIS images (1415 UT and 1555 UT) the probable location of the front line at the surface may be estimated for any time by a simple translation. The subsequent estimated position of the cold front at 1555 UT has been reported in Figure 1. We note that the Polar2 trajectory crossed quasi-perpendicularly the frontal zone first at about 1531 UT during the northward transect, then at about 1551 UT during the return flight toward the way point A.

[18] The meteorological feature described above is confirmed from thermodynamical and dynamical measurements carried out by the Polar2 aircraft during vertical profiles performed in A (warm sector) and B (cold sector) regions (see Figure 1). Figure 3 displays the vertical soundings in warm (A, southern) and cold (B, northern) sectors of the air temperature, the horizontal wind speed and direction. The results clearly show a colder air of about 2°C in the northern sector on all the boundary layer depth (−6°C against −4°C at the cloud top, see Figures 3a and 3d). A strong air temperature inversion is recorded at 830 m at both sectors topping therefore the whole cloud layer at a similar level as reported by the visual observations onboard the aircraft and from satellite information (see Figure 1). Furthermore, the thermodynamical measurement reveals a temperature decrease which is very near the pseudo-adiabatic lapse rate in the cloud layer confirming well-mixed cloud. A same vertical gradient of the horizontal wind speed (12–15 m/s, see Figures 3b and 3e) is observed in both sectors, while a more northward oriented wind direction is evidenced in the

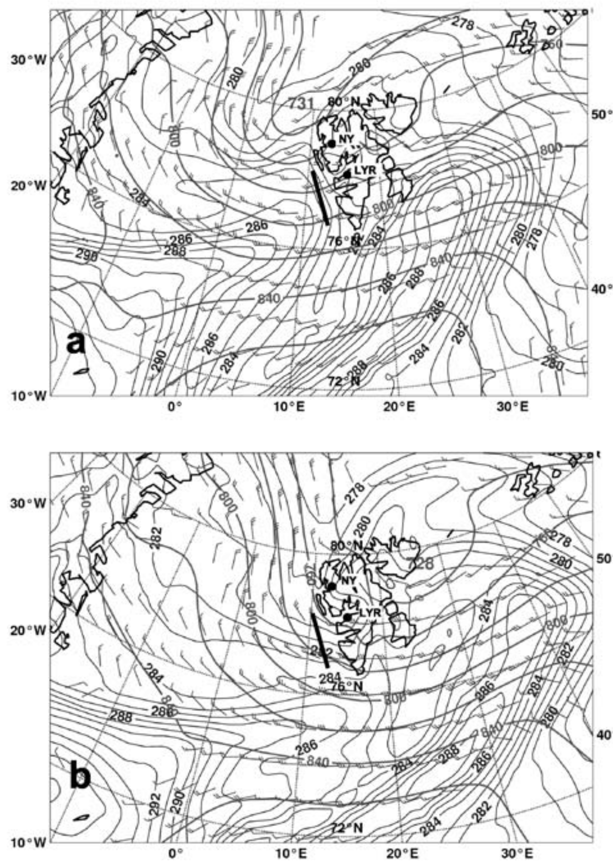

Figure 2. Geopotential, wind vector, and potential temperature fields obtained from the ECMWF analysis at 925 hPa for (a) 1200 UT and (b) 1800 UT. The solid line represents the flight track, and the solid dots represent the locations of Ny-Ålesund (NY) and Longyearbyen (LYR).

cold sector (300° against 260°) confirming that air masses with different thermodynamical properties where sampled when crossing the cold front along the flight transects. We will discuss in the following the microphysical and optical properties of the Arctic cloud layer observed in the warm and cold sectors.

4. Microphysical and Optical Properties of the Boundary Layer Arctic Cloud

4.1. Results Obtained in the Warm Sector

[19] Because no FSSP probe was operated during this flight, the effective droplet diameter and droplet concentration values were estimated by the indirect method which consists to use the LWC and extinction measurements from the Nevzorov and Polar Nephelometer instruments, respectively. The effective diameter can be derived with the following relationship [*Gayet et al.*, 2004]:

$$Deff = A \times \mathrm{LWC}/Ext \tag{1}$$

with *Deff* expressed in μm, LWC in g/m^3, *Ext* in km^{-1} and A = 3000 mm^3/g.

[20] The droplet concentration (N) may therefore be estimated with the following relationships:

$$N = \mathrm{LWC}/\left(\pi/6\rho Deff^3\right) \tag{2}$$

$$\text{or } N = Ext/\left(\varepsilon\pi/4Deff^2\right) \tag{3}$$

with ρ and ε the water density and the extinction efficiency (= 2), respectively. The uncertainties being 15% and 25% on the Nevzorov LWC and Polar Nephelometer extinction measurements (see section 2.1), the subsequent "root-sum-square" (RSS) errors of these uncertainty contributions lead to effective diameter and droplet concentration uncertainties of about 30% and 60%, respectively.

[21] Figures 4a–4d represent the vertical profiles of several microphysical parameters obtained by the successive descent and ascent sequences performed in the warm sector. The parameters are (1) the liquid water content measured by the Nevzorov instrument, (2) the cloud droplet concentration and the effective diameter (see above), and (3) the concentration and (4) the mean volume diameter of drops with diameter larger than 50 μm sampled by the Cloud Particle Imager. Some examples of cloud droplets sampled by the CPI at three levels in the cloud are also displayed in Figure 4. The mean values of LWC and standard deviations are shown in Figure 4a with the adiabatic profile (solid line).

[22] Despite the large fluctuations of the considered parameters, mainly due to the natural cloud inhomogeneities, our observations allow to assess the mean feature of the cloud system. The liquid water content (LWC) mainly increases with height up to 0.6 g/m^3 at the cloud top (Figure 4a). The cloud layer is 450 m vertically extended (from 380 m/−2°C to 830 m/−4°C). The comparison between the several profiles carried out in the warm and cold sectors (at the beginning and at the end of the cloud study gives a variation of about 50 m in cloud top altitude.

[23] While the maximum measured values of LWC at all cloud levels agree with estimated adiabatic LWC most of the measured values of LWC are seen to be smaller (see Figure 4a). This suggests that only occasionally small portions of cloud were adiabatic, while on the average (dots) the cloud consisted of subadiabatic LWC particularly in the upper half part of the cloud layer. This feature is mainly caused by significant entrainment processes rather than fractional cloudiness because of its rather high value (~ 90%). The cloud droplet concentration increases with height from 30 cm^{-3} to 55 cm^{-3} at the midcloud depth then exhibits a rather constant value (Figure 4b), whereas the effective diameter increases with the cloud altitude from 20 μm to 26 μm (Figure 4b). Observations during M-PACE experiment [*McFarquhar et al.*, 2007] reported deeper and colder Arctic clouds (−14.5°C on the average versus −6°C this study). Smaller effective diameters were evidenced (from 14 μm to 22 μm on average) whereas the droplet concentrations are of the same order (50 cm^{-3} on average).

[24] The vertical profiles of the concentration and mean volume diameter (MVD) of particles larger than 50 μm (see Figures 4c and 4d), reveal peak concentration of 300 L^{-1} and the largest MVD (about 100 μm) around the middle of

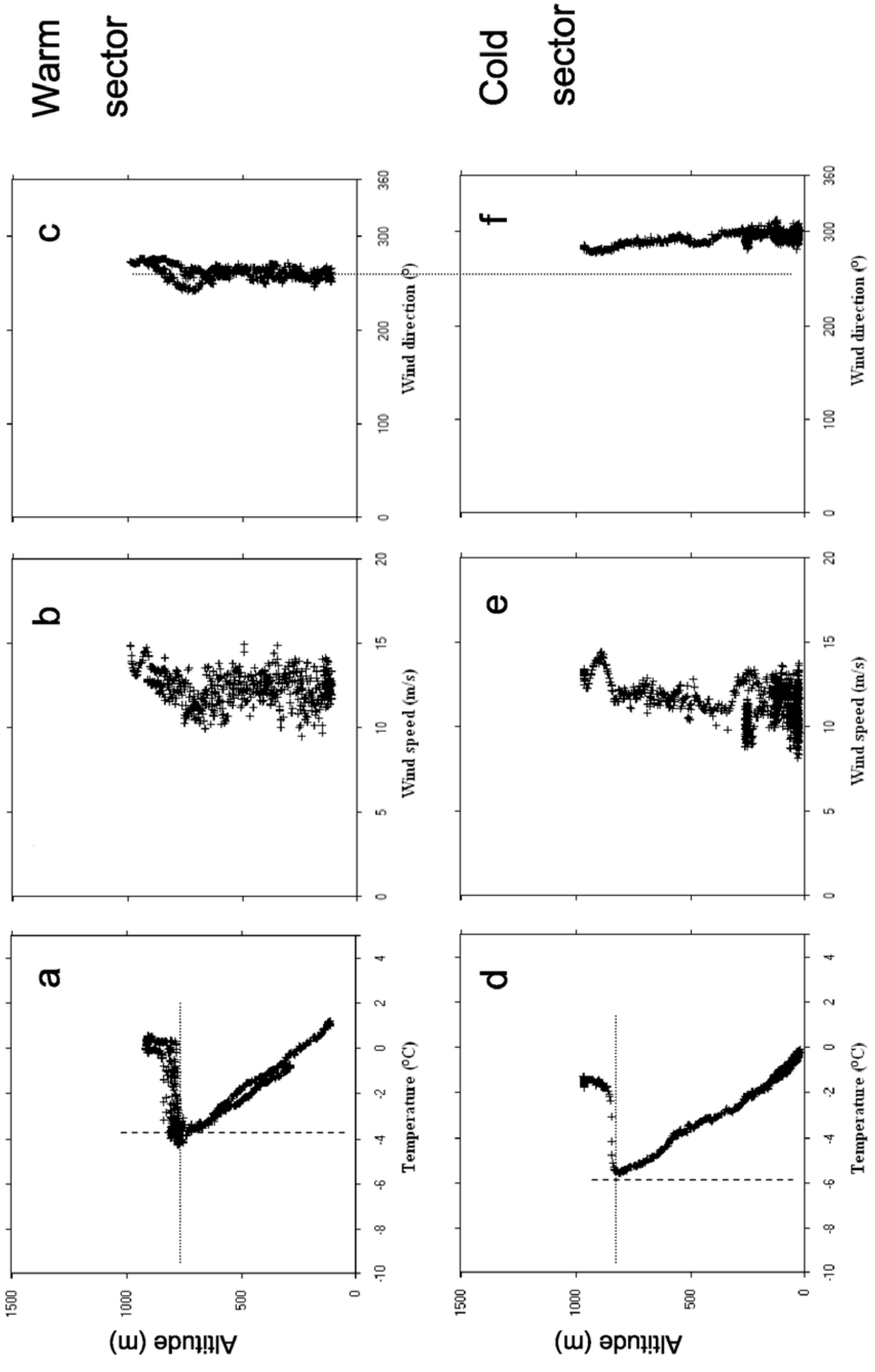

Figure 3. Thermodynamical parameters versus the altitude obtained in (a–c) the warm sector and (bottom) the cold sector. Figures 3a and 3d show air temperature, Figures 3b and 3e show wind speed, and Figures 3c and 3f show wind direction.

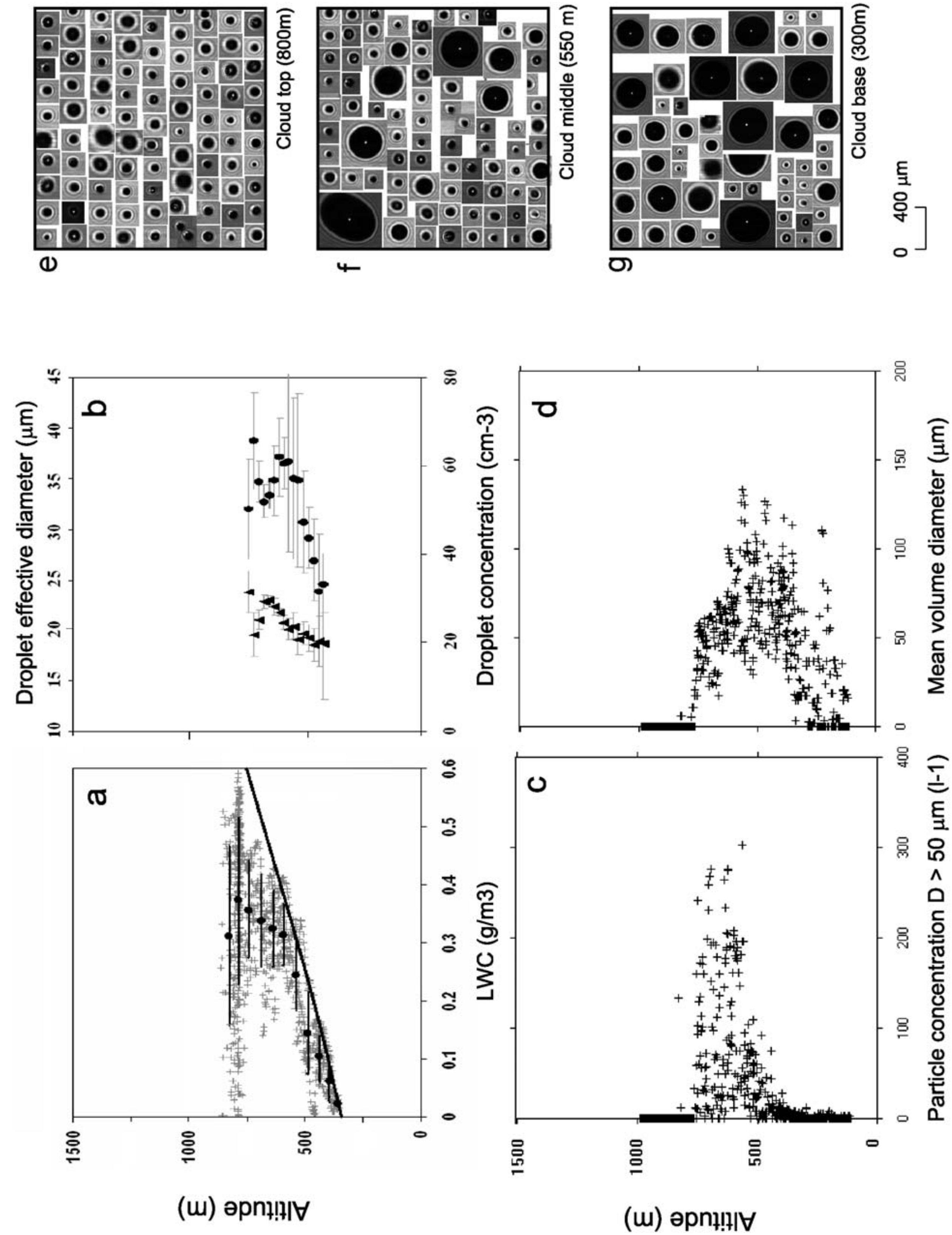
a
Altitude (m)
1500
1000
500
0
0
0.1
0.2
0.3
0.4
0.5
0.6
LWC (g/m3)
b
Droplet effective diameter (µm)
10
15
20
25
30
35
40
45
0
20
40
60
80
Droplet concentration (cm-3)
c
Altitude (m)
1500
1000
500
0
0
100
200
300
400
Particle concentration D > 50 µm (l-1)
d
0
50
100
150
200
Mean volume diameter (µm)
e
Cloud top (800m)
f
Cloud middle (550 m)
g
Cloud base (300m)
0
400 µm

Figure 4

the cloud layer. The analysis of the particle images sampled by the CPI (see examples in Figures 4e–4g) highlight, first, that no ice crystals have been detected at any level in the cloud despite a cloud top temperature of −4°C. The examples of particle images in Figure 4 also illustrate that cloud droplets are observed near to the cloud top, then drizzle drops (due to collision-coalescence processes) are detected with maximum diameter which gradually increases up to 400 μm at lowermost cloud levels. Such big drops can precipitate below the cloud base. We note in passing the CPI drop size distributions did not reveal a bimodal feature as observed by *Lawson et al.* [2001] in similar all water clouds (see Figure A1a).

[25] The low droplet concentration ($\sim$50 cm^{-3}) and the occurrence of drizzle are usual in Arctic boundary layer clouds [see, e.g., *Hobbs and Rangno*, 1998] formed in clean air conditions, i.e., characterized by an aerosol number concentration of about 300 cm^{-3} which was measured by the Polar4 aircraft near the cloud base (see section 5.1).

[26] In the warm sector the cloud properties can be summarized as the following: because of the low concentration ($\sim$ 50 cm^{-3}) of large cloud droplets the collision–coalescence process was effective favoring the drizzle formation with concentration up to 300 L^{-1} (D > 50 μm). Ice particles have not been detected because the cloud top temperature (−4°C) was not low enough to initiate ice nucleation. The cloud can be labeled as cloud type II according to the classification of stratiform clouds in the Arctic by *Rangno and Hobbs* [2001, Figure 9].

4.2. Results Obtained in the Cold Sector

[27] Figures 5a–5e represent the vertical profiles of cloud parameters obtained by successive descent and ascent sequences performed in the northern area within the colder air mass (see Figure 1) about 40 min after the previous cloud sampling. The parameters are (1) the liquid water content and ice water content measured by the Nevzorov and CPI instruments, respectively; (2) the concentration of particles larger than 50 μm; (3) the ice particle shape classification (represented for number and for D > 50 μm); (4) the mean volume diameter of particles with diameter larger than 50 μm; and (5) the concentration of particles larger than 200 μm. These four last parameters were derived from the Cloud Particle Imager data. It should be noticed that because of a failure of the deicing system of the Polar Nephelometer from about 1520 UT the measurements were no longer reliable for the rest of the flight.

[28] Compared to the warm sector sounding, the results in Figure 5 clearly show significant differences in the cloud properties. As highlighted from examples of particle images sampled by the CPI (see Figure 6) ice crystals are observed at any levels in the cloud and no cloud droplets larger than about 50 μm (drizzle) are detected. The cloud microstructure and ice phase are discussed below keeping in mind that the results in Figure 5 do not represent an instantaneous cloud vertical profile because of the high degree of horizontal and vertical heterogeneities for all of the considered parameters.

[29] The LWC profile in Figure 5a reveals peaks and/or traces of liquid water, which were observed at any level in the cloud depth, with a largest LWC value of 0.38 g/m^3 measured 300 m above the cloud base. From the results in Figure 5, it is obviously not possible to identify a well-defined multilayered aspect of the present cloud case. The LWC profile in Figure 5a also shows a significant remnant (up to 0.2 g/m^3) of liquid water in the top of the cloud; which is a common feature observed in mixed phase stratocumulus clouds [*Hobbs and Rangno*, 1998; *Lawson et al.*, 2001; *Gayet et al.*, 2002a; *McFarquhar et al.*, 2007].

[30] As already underlined, ice particles are observed at any cloud level and below the cloud base (precipitation) from the CPI measurements. Because no cloud droplets larger than about 50 μm (drizzle) have been detected, the concentration of particles larger than 50 μm (see Figure 5b) relates ice particle concentration. Obviously ice particles with smallest size occur particularly in ice formation areas [see, e.g., *Lawson et al.*, 2001] but the shape of particles smaller than 50 μm cannot be confidently determined from the analysis of CPI images [*Korolev et al.*, 1999].

[31] The ice particle concentration (D > 50 μm, Figure 5b) is about 40 L^{-1} at the cloud top and reaches 50 L^{-1} near the cloud base. These high ice particle concentrations have already been reported by *Hobbs and Rangno* [1998] and *Rangno and Hobbs* [2001] in Arctic clouds. Quite large ice particles are observed even near the cloud top since the concentration of particles larger than 200 μm are on the order of 7 L^{-1} with median volume diameter of 180 μm. At lower levels the ice particle concentration (D > 200 μm) and MVD increase up to 12 L^{-1} and 370 μm, respectively. The ice water content profile (Figure 5a) reveals values up to 0.25 g/m^3 at the cloud base level.

[32] Because of rather small number of data points, the particle shape classification has been processed every 100 m in order to improve the statistical significance (see Figure 5c). Water droplets are observed in the upper parts of the boundary layer as confirmed by the LWC measurements. Columnar ice crystals dominate the ice particle shape on all the cloud depth and precipitation below as clearly evidenced by CPI examples of ice crystal images in Figure 6. Some graupels are also observed in the lower precipitation levels. Significant differences in ice particle shapes are found with regards to the results by *McFarquhar et al.* [2007] who observed mostly rosette shape in lower cloud parts. These differences are explained by the different temperature ranges as already noted in section 4.1. The inventory of the ice particles types on the average and refined by human classification can be summarized as follow (see also examples of particle images in Figure 6): 32% of pristine columns and needles, 13% of assemblage of columns and 55% of nonpristine ice crystals

Figure 4. Microphysical and optical cloud parameters versus the altitude obtained in the cloud layer in the warm sector: (a) liquid water content measured by the Nevzorov instrument, (b) droplet concentration (solid triangles) and effective diameter (solid circles), (c) concentration of particles with diameter larger than 50 μm (CPI), and (d) mean volume diameter of particles D > 50 μm (CPI). (e–g) Examples of cloud particles sampled by the Cloud Particle Imager at three levels in the cloud. Mean values of LWC and standard deviations are displayed in Figure 4a with the adiabatic profile (full curve).

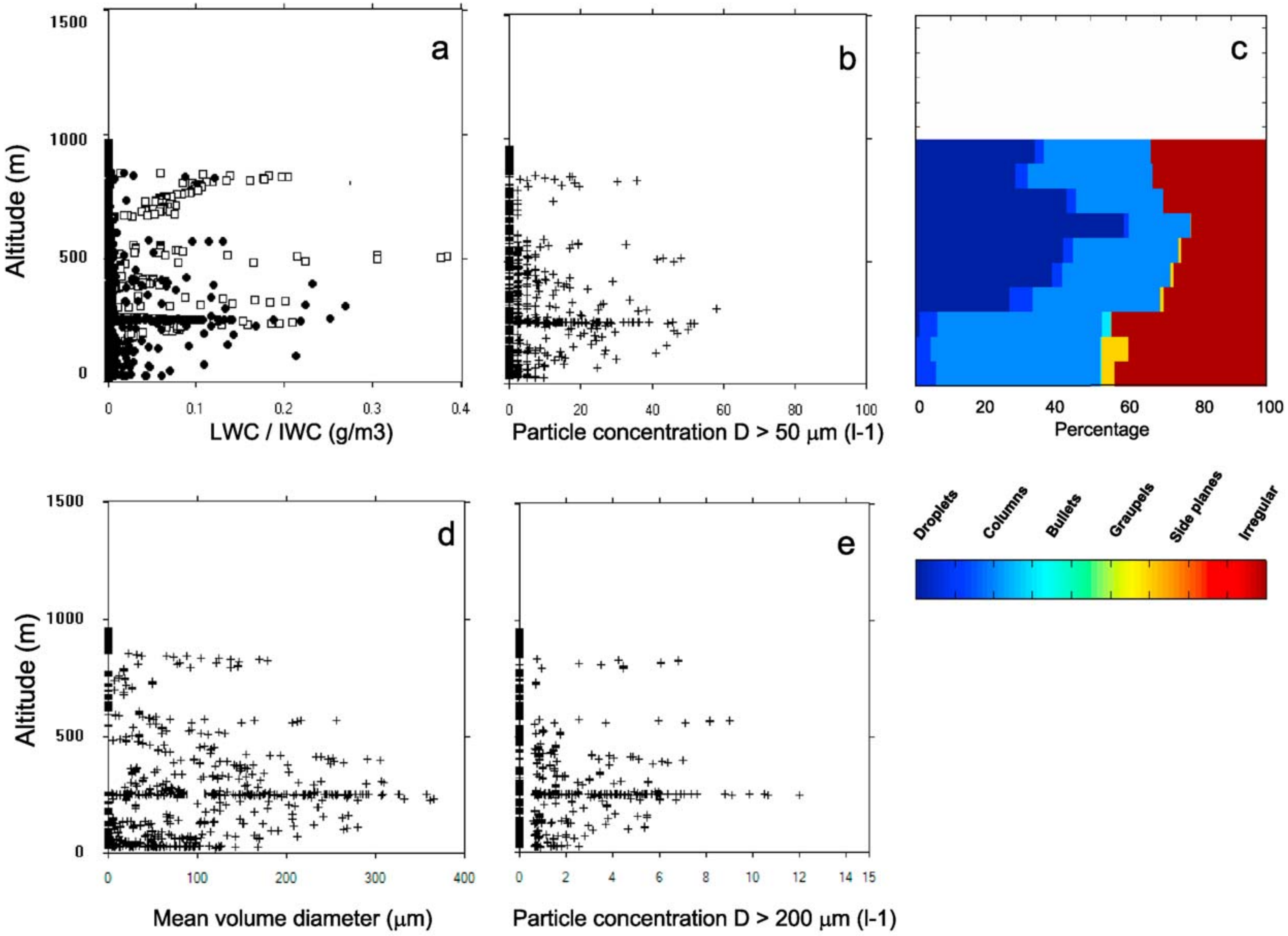

Figure 5. Microphysical and optical cloud parameters versus the altitude obtained in the cloud layer in the cold sector: (a) liquid water content (open squares) and ice water content (solid circles) measured by the Nevzorov and CPI instruments, respectively. (b) Concentration of particles with diameter larger than 50 μm (CPI). (c) The CPI ice particle shape classification (represented for number and for $D > 50$ μm). (d) Mean volume diameter of particles $D > 50$ μm (CPI). (e) Concentration of particles with diameter larger than 200 μm (CPI).

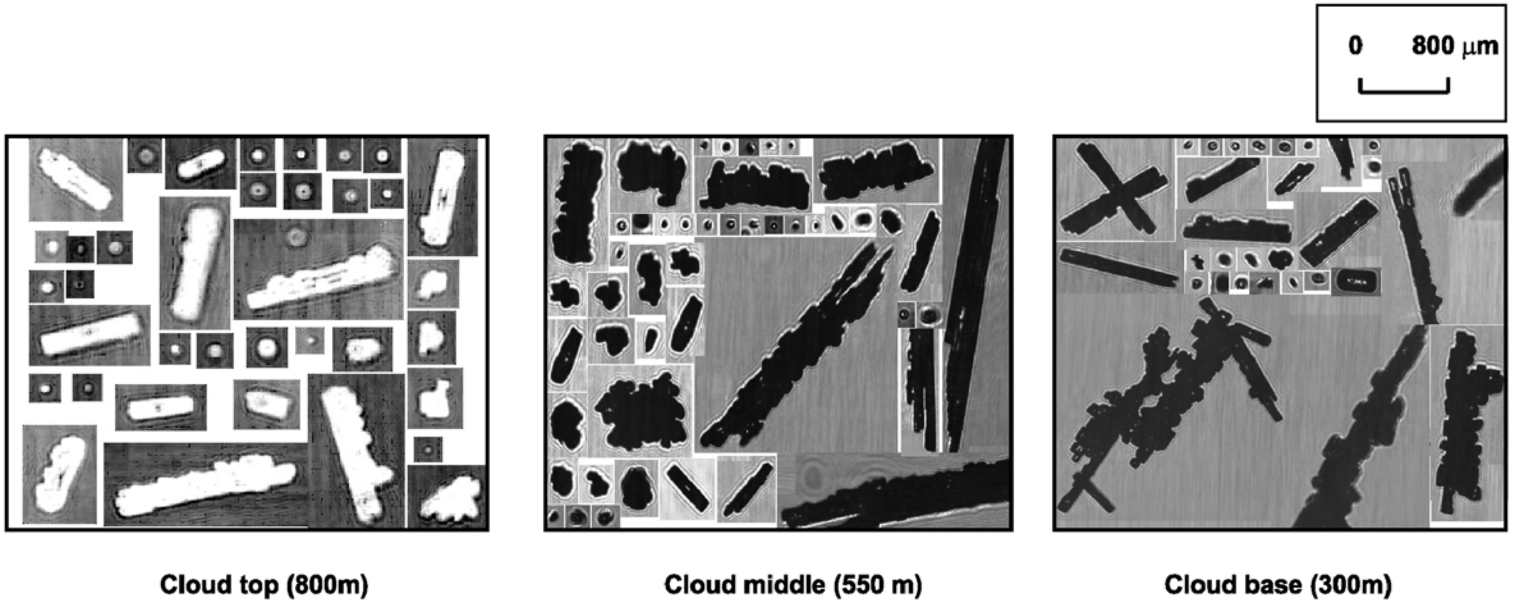

Figure 6. Examples of cloud particles sampled by the Cloud Particle Imager at three cloud levels in the cold sector.

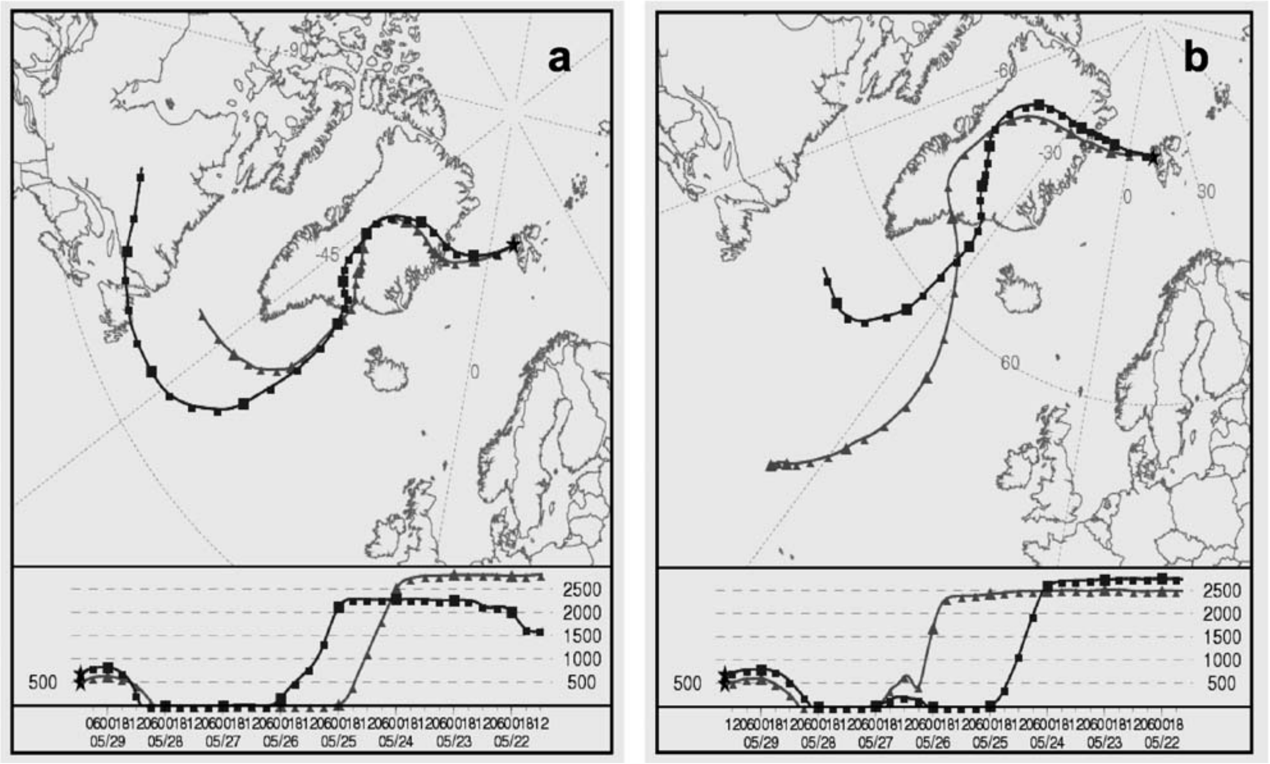

Figure 7. Eight day backward trajectories with starting point at Ny-Ålesund at altitudes 500 m and 700 m: (a) at 1100 UT (warm sector) and (b) at 1500 UT (cold sector) calculated with the NOAA HYSPLIT model.

(irregularly shaped). About 20% of all the ice particles seen on the CPI were rimed (graupels and rimed columns).

[33] According to our observations and following the review from *Rangno and Hobbs* [2001] the stratiform cloud in the postfrontal northern area can be classified as cloud type III [see *Rangno and Hobbs*, 2001, Figure 9]. It should be noticed that neither the observations performed on board the aircraft nor the satellite imagery (NOAA/AVHRR, MODIS) revealed cirrus clouds above the sampling area.

5. Possible Mechanisms to Explain the Observed High Ice Particle Concentrations

5.1. Origin of the Air Masses in the Warm and Cold Sectors

[34] Our observations highlight a quite sharp and clear horizontal difference of cloud top temperatures between the prefrontal warm cloud layer characterized by only supercooled droplets and drizzle (−4°C) and the postfrontal cold cloud with high ice particle concentration (−6°C). Such a temperature threshold at −4°C on the onset of the ice phase has already been noted by *Rangno and Hobbs* [2001] in slightly supercooled stratiform clouds in Arctic [see *Rangno and Hobbs*, 2001, Figure 1], but no correlations with aerosol properties were drawn.

[35] During the ASTAR campaign neither ice nuclei (IN) nor cloud condensation nuclei (CCN) measurements were carried out on board the aircraft and at the Mount Zeppelin station. Therefore, the back trajectory analysis may give some insight about the origin of the air mass in both clouds. The NOAA Hybrid Single-Particle Lagrangian Integrated Trajectory model (HYSPLIT, provided by the Air Resources Laboratory [*Draxler and Rolph*, 2003]) was used to compute 8 day backward trajectories at 1100 UT and 1500 UT (Ny Ålesund starting at 500 m and 700 m, see Figure 1). The results are displayed in Figures 7a and 7b and are related to the warm and cold sectors, respectively (we recall the front passed at around 1300 UT). The analysis of Figure 7 reveals that the air mass traveled over 8 days mainly over the North Atlantic Ocean and middle Greenland to Spitsbergen. Similar features were obtained for higher altitudes above the cloud top (1500 m). These results indicate no significant differences between the origin of the air masses in the warm and cold sector. Despite the inherent limitations in the reliability of the results (particularly for the low levels in the boundary layer, i.e., the clouds in cold and warm sectors may process the aerosol differently before it reaches the points of measurement) the analyzed backward trajectories, at least, provide some basis for speculation about similar IN.

[36] The aerosol measurements performed at the Mount Zeppelin station confirm the above findings in terms of aerosol properties as no differences in aerosol characteristics are determined. The aerosol number density prior to the front was between 300 and 500 cm^{-3}. The size distribution was about evenly divided between the Aitken and accumulation mode particles. When the cold front passed (~1300 UT) significant ice precipitations were recorded (from ground-based micropulse lidar) causing a subsequent reduction of the aerosol number density to ~100 cm^{-3} likely by scavenging processes. Furthermore observations performed near coastal regions showed that only these regions may be influenced by specific circulations with subsequent enhanced entrainment

of ice nuclei aloft to explain appreciable ice water path [*Prenni et al.*, 2007].

[37] The Polar4 aerosol data cannot be reliably used for a detailed description of the aerosol properties regarding the differences between the warm and cold sectors. The icing of the forward facing aerosol inlet during in cloud sequences seriously hampered the data interpretation. Nevertheless, some insights may be derived from the filter analysis, at least in the warm sector before icing. There were stronger contributions from supermicron sea salt particles especially in the lowest few hundred meters above sea surface. Otherwise ammonium sulphate particles constantly dominated the accumulation mode particles ($0.1 < D < 1$ μm). Few mineral dust particles were also spotted and soot particles were suggested to be immersed in some of the sulphate particles as internal mixtures. An aerosol concentration ($D > 13$ nm) about 300 cm^{-3} was measured near the cloud base (before icing), a value close to the measurement made at the Mount Zeppelin station. This value reflects clean air conditions and determines cloud properties with subsequent large diameters (20–26 μm) and low concentrations ($\sim$ 50 cm^{-3}) of cloud droplets.

[38] In conclusion, the analysis of the results of the back trajectory modeling does not reveal significant differences in the origin of the air masses in the warm and cold clouds that might have contributed to differentiate aerosol composition and thus cloud properties. Aerosol-like IN particles do not found favorable conditions to be efficiently activated in the warm sector whereas the thermodynamical conditions in the cold cloud may favor ice nucleation. Therefore a cloud top temperature colder than −4°C appears to be required for the onset of the ice phase in this boundary layer cloud as already noted by *Rangno and Hobbs* [2001] in slightly supercooled stratiform clouds in Arctic.

5.2. Suggested Mechanisms to Explain Ice Enhancement

[39] Many processes controlling ice nucleation remain poorly understood [see, e.g., *Cantrell and Heymsfield*, 2005], and large discrepancies are reported between theory and measurements in clouds warmer than about −15°C with much more ice observed than predicted from different mechanisms. There were a number of recent modeling studies devoted to explore these mechanisms. For example, *Fridlind et al.* [2007] showed that the formation of ice nuclei from drop evaporation residuals and drop freezing during evaporation could be invoked to explain why ice crystal concentrations are greater than ice nuclei concentrations. *Sednev et al.* [2008] demonstrated that the Bergeron-Findeisen process mainly explained the glaciation of supercooled clouds, and *Morrison et al.* [2008] described that the response of mixed phase Arctic clouds to increased aerosol concentrations depends in part on the underlying surface conditions.

[40] The observations reported here confirm high ice particle concentrations (up to 50 L^{-1}) even with rather warm cloud top (−6°C) compared to the above previous studies. According to the ice crystals shapes and thermodynamical characteristics, two main mechanisms for ice enhancement may be hypothesized in order to explain our observations, namely: the shattering of large drops during freezing [see, e.g., *Griggs and Choularton*, 1983] and the ice splinter production during riming (so-called Hallett-Mossop process [*Hallett and Mossop*, 1974]). We note that a careful analysis of the relative trajectories (in a Lagrangian reference) of both Polar2 and Polar4 aircraft did definitively reject the possibility of aircraft producing abnormal high concentration of small ice crystals when passing trough the clouds (caused by the rapid expansion and the subsequent cooling by the propeller rotation) as reported by *Rangno and Hobbs* [1983].

[41] 1. A general consensus was found about the mechanism of shattering of large drops during freezing that as many as about 10% of drops larger than 50 μm may shatter in the temperature range −5 to −15°C. This mechanism could operate because large supercooled drops and drizzle are present before the onset of the ice phase. Once the ice has formed the absence of such large drops may also indicate that drizzle drops to shatter during freezing. Therefore part of the expected ice fragments produced by the shattering of isolated large drops during freezing may be attributed to the observed ice particles with irregular shapes. Since 55% of ice particles ($D > 50$ μm) have been recognized as irregularly shaped the shattering of isolated drops made a significant contribution in high ice concentrations. The subsequent concentration of such ice particles is about 27 L^{-1}.

[42] 2. There are several thermodynamical and microphysical characteristics in favor of the operation of the Hallett-Mossop process. First, the high concentrations of ice particles are found inside the operational range of temperature (between −4°C and −6°C). Second, our observations evidence broadened size distribution of the supercooled droplets (with diameters up to 200–300 μm as evidenced by CPI images in Figure 4) with quite large effective diameter (Deff = 26 μm, see section 4.1) and the occurrence of large rimed columnar ice crystals (see Figure 6). The rate of splinter production per second (r) can be estimated from the following relationship [*Willis and Hallett*, 1991]:

$$\mathrm{r = NgNdVg\pi D^2E/800} \qquad (4)$$

with Ng the concentration of riming particles (i.e., single columnar ice crystals with $D > 200$ μm: 3 L^{-1}), Nd the concentration of drops > 23 μm (estimated to 10 cm^{-3}), Vg the terminal velocity of columns (0.7 m/s), D the diameter of the riming particles (1 mm) and E the collection efficiency (assumed to 0.5). The result of the calculation gives a rate of splinters of 0.04 $\text{L}^{-1}\text{s}^{-1}$ or a crystal concentration of 24 L^{-1} assuming the cloud microstructure remains constant during 10 min. Of course there are very large uncertainties on these estimated values. The "root-sum-square" (RSS) errors of the contributions of all uncertainties on the measurements in equation (4) lead to an error of about 120%. Nevertheless, an ice crystal concentration of 24 L^{-1} is of the same order of magnitude of the concentration of pristine columns ($D > 50$ μm) observed in the cloud (up to 16 L^{-1}) and accounting for about 32% of the ice particles (see section 4.2). Therefore the production of ice splinters by riming might contribute to the observed high ice concentration in the cloud.

[43] We note in passing the fragmentation of ice crystals by collisions was already evidenced to be efficient in Arctic clouds as reported by *Schwarzenboeck et al.* [2009].

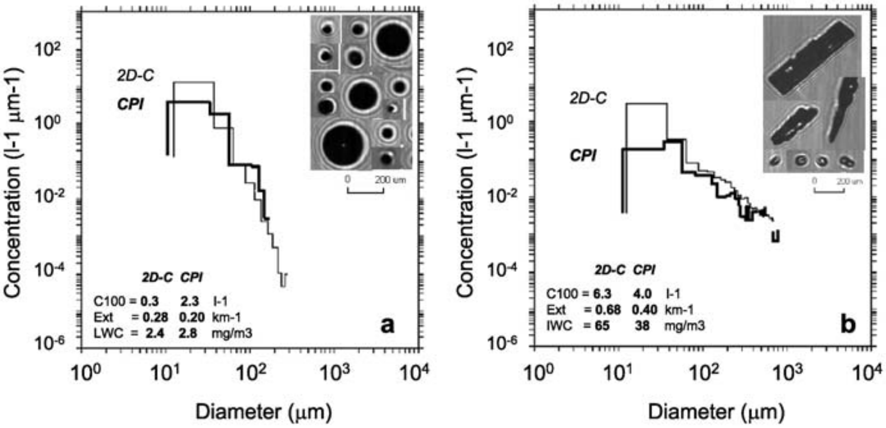

Figure A1. Mean particle size distributions measured by the 2D-C and the CPI probes obtained in (a) the warm and (b) the cold sectors. Mean values of the concentration of particles with D > 100 μm, extinction coefficient and ice water content are also depicted.

Although pristine and delicate crystals have been observed here the few fragments of ice crystals recognized account for a noneffective fragmentation process.

6. Conclusions

[44] In this paper we present the results of a case study (29 May, 2004) during the ASTAR airborne campaign in the vicinity of the west coast of the Svalbard Archipelago. The synoptic observations showed a cold front passing the observation area associated with typical Arctic boundary layer stratiform cloud system. The cold front line was identified from the analyses of satellite images and from observations at Ny-Ålesund and Zeppelin Mountain stations and from airborne thermodynamical measurements. The cloud measurements have been performed in both warm and cold sectors regarding the cold front line and significant differences have been evidenced in the cloud microstructure accordingly.

[45] In the warm sector of the low-pressure system with a cloud top temperature at −4°C no ice particles were detected. The cloud layer was 450 m vertically extended (from 380 m to 830 m). Occasionally were small portions of cloud adiabatic, while on the average the cloud consisted of subadiabatic LWC particularly in the upper half part of the cloud layer. An aerosol number concentration of about 300 cm^{-3} measured near the cloud base reveals a cloud formation in clear air conditions with subsequent large effective diameter (20–26 μm) and low concentration (50 cm^{-3}) of cloud droplets. Therefore, the collision–coalescence process was effective favoring the drizzle formation with concentration up to 300 L^{-1} (D > 50 μm). Compared to *Rangno and Hobbs*'s [2001] observations the cloud properties measured in the warm sector are comparable with their type II clouds.

[46] In the cold sector behind the frontal zone, with a lower cloud top temperature (−6°C), ice crystals were observed in the entire cloud layer and no cloud droplets larger than about 50 μm (drizzle) were detected. The increased ice particle concentrations reported (up to 50 L^{-1}) are much higher than ice nucleus concentrations expected in Arctic regions. The shattering of isolated drops during freezing and the ice splinter production during riming appears one of the most likely processes to explain the observations of high ice concentration. The cloud properties and subsequent ice production mechanisms evidenced in Svalbard are quite comparable with the observations from *Rangno and Hobbs*'s [2001] obtained in similar cloudy conditions (classified as type II) near Barrow (Alaska).

[47] The analysis of the back trajectories does not reveal significant differences in the origin of the air masses in the warm and cold sectors that might have contributed to differentiate aerosol composition and thus cloud properties. Aerosol-like IN particles do not found favorable conditions to be efficiently activated in the warm sector whereas the thermodynamical conditions in the cold cloud may favor ice nucleation. Therefore a cloud top temperature colder than −4°C appears to be required for the onset of the ice phase in this boundary layer cloud as already noted by *Rangno and Hobbs* [2001] in slightly supercooled stratiform clouds in Arctic.

Appendix A: Microphysical Parameters Derived From the CPI Instrument

[48] As indicated in section 2, the 2D-C data were not included in the paper because of some intermittent failures of the data acquisition system. Therefore the CPI data were used in order to derive the particle size distributions and the microphysical parameters as *Gallagher et al.* [2005] in cirrus clouds. Cloud particle sizes, when inferred from images taken with this instrument, are oversized with regards to the true dimension. Furthermore, the subsequent distances on which the particles are accepted in the image frame are greater than the depth of field from the object plane. Therefore, large uncertainties occur on derived size distributions particularly for particles smaller than about 100 μm. In order to reduce these errors, a calibration method was devised [*Connolly et al.*, 2007] from optical bench measurements which use calibrated glass beads and ice analogs. The CPI operated during ASTAR 2004 campaign was calibrated by applying this method at the University of Manchester [*Lefèvre*, 2007]. In order to validate the calibration results the CPI size distributions were compared to available 2D-C

data. Figures A1a and A1b display the results for cloud sequences where the 2D-C worked properly obtained in the warm and cold sectors, respectively. A rather good agreement is found between the two size distributions for both water drops (Figure A1a) and ice crystals (mainly columns, see Figure A1b). Mean values of the concentration of particles with D > 100 μm, extinction coefficient and ice water content are also reported in Figure A1 for both instruments. The discrepancies between the two probes are within the large uncertainties expected for the 2D-C instrument (up to 75% and 100% on particle concentration and ice water content, respectively [see *Gayet et al.*, 2002b]). Therefore, we consider the errors on the size distributions and derived microphysical parameters calculated from the (calibrated) CPI are of the same order of those from the 2D-C.

[49] **Acknowledgments.** This work was funded by the Institut Polaire Français Paul Emile Victor (IPEV) and by a grant from the CNRS/INSU. We thank the members of OPTIMARE GmbH and Deutsches Zentrum für Luft- und Raumfahrt (DLR) who organized the experiment management and aircraft operations. We acknowledge C. Gourbeyre (LaMP) and J.-F. Fournol for their technical assistance. We are grateful to A. Dörnbrack (DLR) for providing meteorological analysis from the ECMWF model. The authors would like to give recognition to G. Mioche, C. Duroure, R. Lefèvre (LaMP), J. Ström (Stockholm University), and A. Minikin (DLR) for helpful discussions. The authors gratefully acknowledge the NOAA Air Resources Laboratory (ARL) for the provision of the HYSPLIT transport and dispersion model and READY Web site (http://www.arl.noaa.gov/ready.html) used in this publication. We thank anonymous reviewers who made important comments which strengthened the manuscript.

References

Arctic Climate Impact Assessment (2004), *Impacts of a Warming Arctic*, 139 pp., Cambridge Univ. Press, New York.

Baker, B., and R. P. Lawson (2006), Improvement in determination of ice water content from two-dimensional particle imagery, part I: Image-to-mass relationships, *J. Appl. Meteorol. Climatol.*, *45*, 1282–1290, doi:10.1175/JAM2398.1.

Cantrell, W., and A. Heymsfield (2005), Production of ice in tropospheric clouds: A review, *Bull. Am. Meteorol. Soc.*, *86*, 795–807, doi:10.1175/BAMS-86-6-795.

Cappelaz, J. A., I. Fung, and A. M. Thompson (1993), The atmospheric CH_4 increase since the Last Glacial Maximum, part I: Source estimates, *Tellus, Ser. B*, *45*, 228–241.

Connolly, P. J., M. J. Flynn, Z. Ulanowski, T. W. Choularton, M. W. Gallagher, and K. N. Bower (2007), Calibration of the cloud particle imager probes using calibration beads and ice crystal analogues: The depth of field, *J. Atmos. Oceanic Technol.*, *24*, 1860–1879, doi:10.1175/JTECH2096.1.

Cooper, W. A. (1977), Cloud physics investigation by the University of Wyoming in HYPLEX 1977, *Rep. AS 119*, 321 pp., Bur. of Reclamation, Washington, D. C.

Curry, J. A., E. E. Ebert, and J. L. Schramm (1993), Impact of clouds on the surface radiation balance of the Arctic Ocean, *Meteorol. Atmos. Phys.*, *51*, 197–217, doi:10.1007/BF01030494.

Curry, J. A., W. B. Rossow, D. Randall, and J. L. Schramm (1996), Overview of Arctic cloud and radiation characteristics, *J. Clim.*, *9*, 1731–1764, doi:10.1175/1520-0442(1996)009<1731:OOACAR>2.0.CO;2.

Dethloff, K., et al. (2006), A dynamical link between the Arctic and the global climate system, *Geophys. Res. Lett.*, *33*, L03703, doi:10.1029/2005GL025245.

Dickson, B., I. Yashayaev, J. Meincke, B. Turrell, S. Dye, and J. Holfort (2002), Rapid freshening of the deep North Atlantic Ocean over the past four decades, *Nature*, *416*, 832–837, doi:10.1038/416832a.

Draxler, R. R., and G. D. Rolph (2003), HYSPLIT (Hybrid Single-Particle Lagrangian Integrated Trajectory) model, Air Resour. Lab., NOAA, Silver Spring, Md. (Available at http://www.arl.noaa.gov/ready/hysplit4.html)

Engvall, A.-C., R. Krejci, J. Ström, R. Treffeisen, R. Scheele, O. Hermansen, and J. Paatero (2008), Changes in aerosol properties during spring-summer period in the Arctic troposphere, *Atmos. Chem. Phys.*, *8*, 445–462.

Field, P. R., A. J. Heymsfield, and A. Bansemer (2006), Shattering and interarrival times measured by optical array probes in ice clouds, *J. Atmos. Oceanic Technol.*, *23*, 1357–1371, doi:10.1175/JTECH1922.1.

Fridlind, A. M., A. S. Ackerman, G. McFarquhar, G. Zhang, M. R. Poellot, P. J. DeMott, A. J. Prenni, and A. J. Heymsfield (2007), Ice properties of single-layer stratocumulus during the Mixed-Phase Arctic Cloud Experiment: 2. Model results, *J. Geophys. Res.*, *112*, D24202, doi:10.1029/2007JD008646.

Gallagher, M. W., P. J. Connolly, J. Whiteway, D. Figuera-Nieto, M. Flynn, T. W. Choularton, K. N. Bower, C. Cook, R. Busen, and J. Hacker (2005), An overview of the microphysical structure of cirrus clouds observed during EMERALD-1, *Q. J. Meteor. Soc.*, *131*, 1143–1169, doi:10.1256/qj.03.138.

Gayet, J. F., O. Crépel, J. F. Fournol, and S. Oshchepkov (1997), A new airborne polar nephelometer for the measurements of optical and microphysical cloud properties, part I: Theoretical design, *Ann. Geophys.*, *15*, 451–459, doi:10.1007/s00585-997-0451-1.

Gayet, J.-F., S. Asano, A. Yamazaki, A. Uchiyama, A. Sinyuk, O. Jourdan, and F. Auriol (2002a), Two case studies of winter continental-type water and mixed-phase stratocumuli over the sea: 1. Microphysical and optical properties, *J. Geophys. Res.*, *107*(D21), 4569, doi:10.1029/2001JD001106.

Gayet, J.-F., F. Auriol, A. Minikin, J. Ström, M. Seifert, R. Krejci, A. Petzold, G. Febvre, and U. Schumann (2002b), Quantitative measurement of the microphysical and optical properties of cirrus clouds with four different in situ probes: Evidence of small ice crystals, *Geophys. Res. Lett.*, *29*(24), 2230, doi:10.1029/2001GL014342.

Gayet, J.-F., J. Ovarlez, V. Shcherbakov, J. Ström, U. Schumann, A. Minikin, F. Auriol, A. Petzold, and M. Monier (2004), Cirrus cloud microphysical and optical properties at southern and northern midlatitudes during the INCA experiment, *J. Geophys. Res.*, *109*, D20206, doi:10.1029/2004JD004803.

Griggs, D. J., and T. W. Choularton (1983), Freezing modes of riming droplets with application to ice splinter production, *Q. J. R. Meteorol. Soc.*, *109*, 243–253.

Hallett, J., and S. C. Mossop (1974), Production of secondary particles during the riming process, *Nature*, *249*, 26–28, doi:10.1038/249026a0.

Hegg, D. A., P. V. Hobbs, S. Gasso, J. D. Nance, and A. L. Rangno (1996), Aerosol measurements in the Arctic relevant to direct and indirect radiative forcing, *J. Geophys. Res.*, *101*, 23,349–23,363, doi:10.1029/96JD02246.

Heymsfield, A. J. (2007), On measurements of small ice particles in clouds, *Geophys. Res. Lett.*, *34*, L23812, doi:10.1029/2007GL030951.

Hobbs, P. V., and A. L. Rangno (1998), Microstructure of low and middle-level clouds over the Beaufort Sea, *Q. J. R. Meteorol. Soc.*, *124*, 2035–2071, doi:10.1002/qj.49712455012.

Intergovernmental Panel on Climate Change (IPCC) (2007), *Climate Change 2007—The Fourth Assessment Report of the IPCC*, Cambridge Univ. Press, Cambridge, U. K.

Korolev, A., and G. A. Isaac (2005), Shattering during sampling by OAPs and HVPS. Part I: Snow particles, *J. Atmos. Oceanic Technol.*, *22*, 528–543, doi:10.1175/JTECH1720.1.

Korolev, A. V., J. W. Strapp, G. A. Isaac, and A. N. Nevzorov (1998), The Nevzorov airborne hot-wire LWC-TWC probe: Principle of operation and performance characteristics, *J. Atmos. Oceanic Technol.*, *15*(6), 1495–1510, doi:10.1175/1520-0426(1998)015<1495:TNAHWL>2.0.CO;2.

Korolev, A. V., G. A. Isaac, and J. Hallet (1999), Ice particle habits in Arctic clouds, *Geophys. Res. Lett.*, *26*, 1299–1302, doi:10.1029/1999GL900232.

Lawson, R. P., and B. A. Baker (2006), Improvement in determination of ice water content from two-dimensional particle imagery, part II: Applications to collected data, *J. Appl. Meteorol.*, *45*(9), 1291–1303, doi:10.1175/JAM2399.1.

Lawson, R. P., B. A. Baker, and C. G. Schmitt (2001), An overview of microphysical properties of Arctic clouds observed in May and July 1998 during FIRE ACE, *J. Geophys. Res.*, *106*, 14,989–15,014.

Lawson, R. P., D. O'Connor, P. Zmarzly, K. Weaver, B. A. Baker, Q. Mo, and H. Jonsson (2006), The 2D-S (Stereo) probe: Design and preliminary tests of a new airborne, high speed, high-resolution particle imaging probe, *J. Atmos. Oceanic Technol.*, *23*, 1462–1477, doi:10.1175/JTECH1927.1.

Lefèvre, R. (2007), Physique de la mesure de la sonde CPI. Application à la campagne ASTAR, thesis, 187 pp., Univ. Blaise Pascal, Aubière, France.

Lubin, D., and A. M. Vogelmann (2006), A climatologically significant aerosol longwave indirect effect in the Arctic, *Nature*, *439*, 453–456, doi:10.1038/nature04449.

McFarquhar, G., G. Zhang, M. R. Poellot, G. L. Kok, R. McCoy, T. Tooman, A. Fridlind, and A. Heymsfield (2007), Ice properties of single-layer stratocumulus during the Mixed-Phase Arctic Cloud Experiment: 1. Observations, *J. Geophys. Res.*, *112*, D24201, doi:10.1029/2007JD008633.

Morrison, H., M. D. Shupe, J. O. Pinto, and J. D. Curry (2005), Possible roles of ice nucleation mode and ice nuclei depletion in the extended lifetime of Arctic mixed-phase clouds, *Geophys. Res. Lett.*, *32*, L18801, doi:10.1029/2005GL023614.

Morrison, H., J. O. Pinto, J. A. Curry, and G. McFarquhar (2008), Sensitivity of modeled arctic mixed-phase stratocumulus to cloud condensation and ice nuclei over regionally varying surface conditions, *J. Geophys. Res.*, *113*, D05203, doi:10.1029/2007JD008729.

Prenni, A. J., J. Y. Harrington, M. Tjernström, P. J. DeMott, A. Avramov, C. N. Long, S. M. Kreidenweis, P. Q. Olsson, and J. Verlinde (2007), Can ice-nucleating aerosols affect Arctic seasonal climate?, *Bull. Am. Meteorol. Soc.*, *88*, 541–550, doi:10.1175/BAMS-88-4-541.

Rangno, A. L., and P. V. Hobbs (1983), Production of ice particles in clouds due to aircraft penetrations, *J. Clim. Appl. Meteorol.*, *22*, 214–232, doi:10.1175/1520-0450(1983)022<0214:POIPIC>2.0.CO;2.

Rangno, A. L., and P. V. Hobbs (2001), Ice particles in stratiform clouds in the Arctic and possible mechanisms for the production of high ice concentration, *J. Geophys. Res.*, *106*, 15,065–15,075, doi:10.1029/2000JD900286.

Rossow, W. B., A. W. Walker, and L. C. Garder (1993), Comparison of ISCCP cloud detection, *J. Clim.*, *6*, 2370–2393, doi:10.1175/1520-0442(1993)006<2370:VOICD>2.0.CO;2.

Sassen, K. (2005), Dusty ice clouds over Alaska, *Nature*, *434*, 456, doi:10.1038/434456a.

Schwarzenboeck, A., V. Shcherbakov, R. Lefèvre, J.-F. Gayet, C. Duroure, and Y. Pointin (2009), Evidence for stellar-crystal fragmentation in Arctic clouds, *Atmos. Res.*, *92*, 220–228, doi:10.1016/j.atmosres.2008.10.002.

Sednev, I., S. Menon, and G. McFarquhar (2008), Simulating mixed-phase Arctic stratus clouds: Sensitivity to ice initiation mechanisms, *Atmos. Chem. Phys. Discuss.*, *8*, 11,755–11,819.

Verlinde, J., et al. (2007), The mixed-phase Arctic cloud experiment (M-PACE), *Bull. Am. Meteorol. Soc.*, *88*, 205–221, doi:10.1175/BAMS-88-2-205.

Willis, P. T., and J. Hallett (1991), Microphysical measurements from an aircraft ascending with a growing isolated maritime cumulus tower, *J. Atmos. Sci.*, *48*, 283–299, doi:10.1175/1520-0469(1991)048<0283:MMFAAA>2.0.CO;2.

Winker, D., and C. Trepte (2007), Distribution and characteristics of polar clouds from CALIOP, paper presented at A-Train Lille 07 Symposium, Cent. Natl. d'Études Spatiales, Lille, France, 22–25 Oct.

Zuidema, P., B. Baker, Y. Han, J. Intrieri, J. Key, P. Lawson, S. Matrosov, M. Shupe, R. Stone, and T. Uttal (2005), An Arctic springtime mixed-phase cloudy boundary layer observed during SHEBA, *J. Atmos. Sci.*, *62*, 160–176, doi:10.1175/JAS-3368.1.

J. Bareiss and A. Helbig, Department of Environmental Meteorology, University of Trier, D-54286 Trier, Germany.

J.-F. Gayet and A. Schwarzenboeck, Laboratoire de Météorologie Physique, UMR 6016, Université Blaise Pascal, CNRS, F-63177 Aubière, France. (gayet@opgc.univ-bpclermont.fr)

A. Herber and R. Treffeisen, Alfred Wegener Institute for Polar and Marine Research, D-27515 Bremerhaven, Germany.

A. Matsuki, Frontier Science Organization, Kanazawa University, Kanazawa 920-1192, Japan.